

Structure-Guided Design, Synthesis, and Biological Evaluation of Peripheral Anionic Site Selective and Brain Permeable Novel Oxadiazole-Piperazine Conjugates against Alzheimer's Disease with Antioxidant Potential

Abhinav Singh, Akash Verma, Bhagwati Bhardwaj, Poorvi Saraf, Hansal Kumar, Nishi Jain, Digambar Kumar Waiker, T A Gajendra, Sairam Krishnamurthy, and Sushant K. Shrivastava*



Cite This: *ACS Omega* 2024, 9, 18169–18182



Read Online

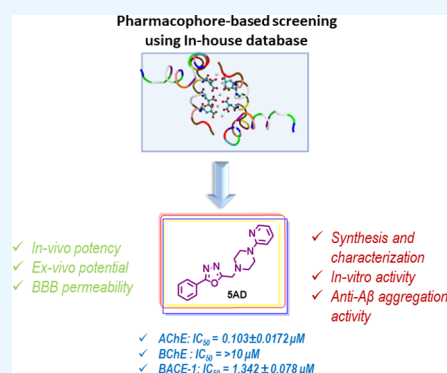
ACCESS |

Metrics & More

Article Recommendations

Supporting Information

ABSTRACT: Alzheimer's disease (AD) is a multifactorial and emerging neurological disorder, which has invoked researchers to develop multitargeted ligands. Herein, hybrid conjugates of 5-phenyl-1,3,4-oxadiazole and piperazines were rationally designed, synthesized, and pharmacologically evaluated against hAChE, hBChE, and hBACE-1 enzymes for the management of AD. Among the series, compound **5AD** comprising pyridyl substitution at terminal nitrogen of piperazine contemplated as a paramount lead compound (hAChE, $IC_{50} = 0.103 \pm 0.0172 \mu\text{M}$, hBChE, $IC_{50} \geq 10 \mu\text{M}$, and hBACE-1, $IC_{50} = 1.342 \pm 0.078 \mu\text{M}$). Compound **5AD** showed mixed-type enzyme inhibition in enzyme kinetic studies against the hAChE enzyme. In addition, compound **5AD** revealed a significant displacement of propidium iodide from the peripheral anionic site (PAS) of hAChE and excellent blood–brain barrier (BBB) permeability in a parallel artificial membrane permeation assay (PAMPA). Besides, **5AD** also exhibited anti- $A\beta$ aggregation activity in self- and AChE-induced thioflavin T assay. Further, compound **5AD** has shown significant improvement in learning and memory ($p < 0.001$) against the in vivo scopolamine-induced cognitive dysfunction mice model. The ex vivo study implied that after treatment with compound **5AD**, there was a decrease in AChE and malonaldehyde (MDA) levels with an increase in catalase (CAT, oxidative biomarkers) in the hippocampal brain homogenate. Hence, compound **5AD** could be regarded as a lead compound and further be explored in the treatment of AD.



1. INTRODUCTION

Alzheimer's disease (AD) is the most common neurodegenerative disease in adults characterized by progressive and irreversible memory decline, which mainly manifests cognitive impairment, behavioral change, and memory loss, which develops socioeconomic burden to the developing countries.^{1,2} As per the World's Alzheimer's report 2021, the number of individuals affected with AD will rise from 35 million to 135 million by 2050.³ AD is a multifactorial progressive disorder characterized by various pathological hallmarks such as a downregulation in the AChE level causing synaptic plasticity, tau hyperphosphorylation, deposition and aggregation of $A\beta$,⁴ formation of neurofibrillary tangles (NFTs),⁵ N-methyl-D-aspartate receptor (NMDAR) activation disturbing synaptic transmission,⁶ neuronal cell apoptosis with CNS inflammation,⁷ cAMP response element-binding protein signaling mechanism associated with gene transcription,⁸ and ROS production via oxidative stress damage. The current FDA-approved drugs include AChE inhibitors (donepezil, rivastigmine, and galantamine) and NMDAR antagonists (memantine) are only used for symptomatic treatment without

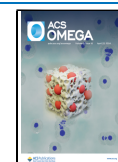
addressing the disease progression.⁹ However, these are acting toward their specific target, namely, cholinesterases, thus having several difficulties specifically metabolic changes, drug–drug interaction, optimum plasma drug concentration problems, and compatibility of dosage form with patients.¹⁰ The conventional approach of drug designing involves targeting a protein with a single molecule, which has several adverse effects leading to failure at the inception. Indeed, the approaches to designing a molecule have been shifted to multitargeted agents to combat this multifactorial disease^{11,12} and recently implemented multifunctional ligand designing (MTDL) strategies made us inquisitive to design a molecule that could simultaneously aim multiple pathogenic targets in AD.^{13,14} Therefore, multitargeted therapeutics with the

Received: December 22, 2023

Revised: March 20, 2024

Accepted: March 22, 2024

Published: April 11, 2024



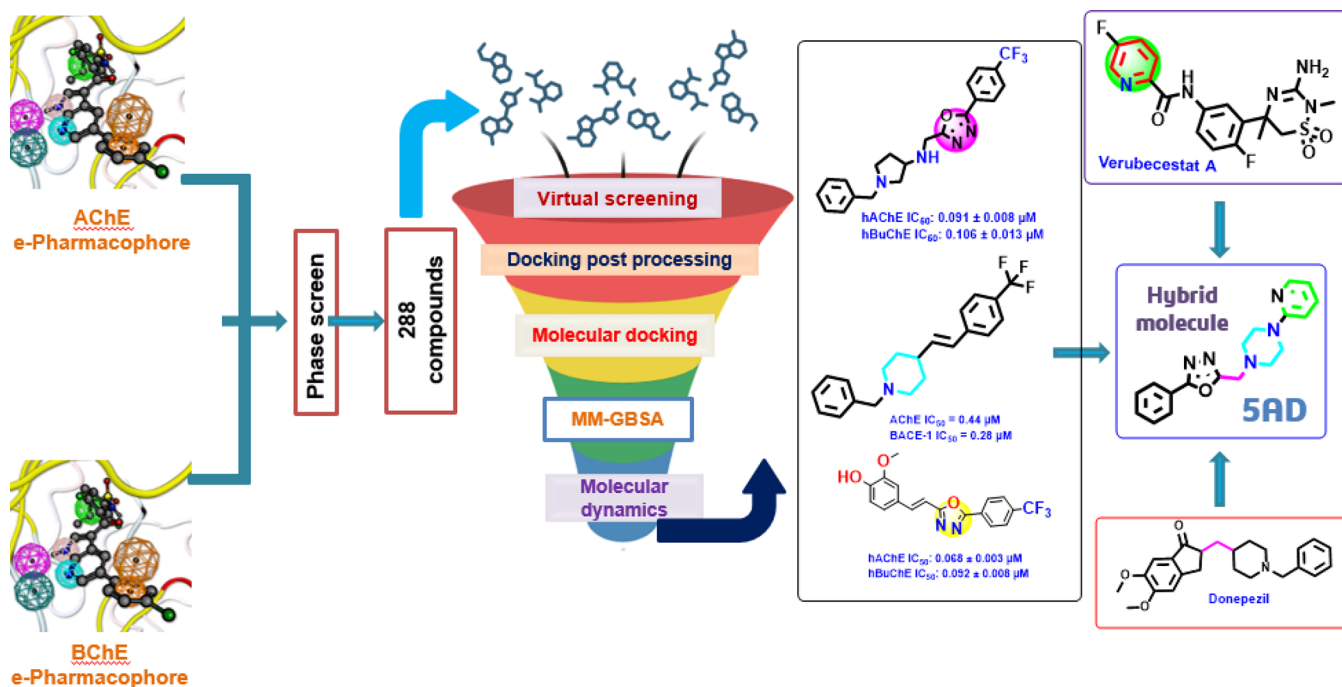
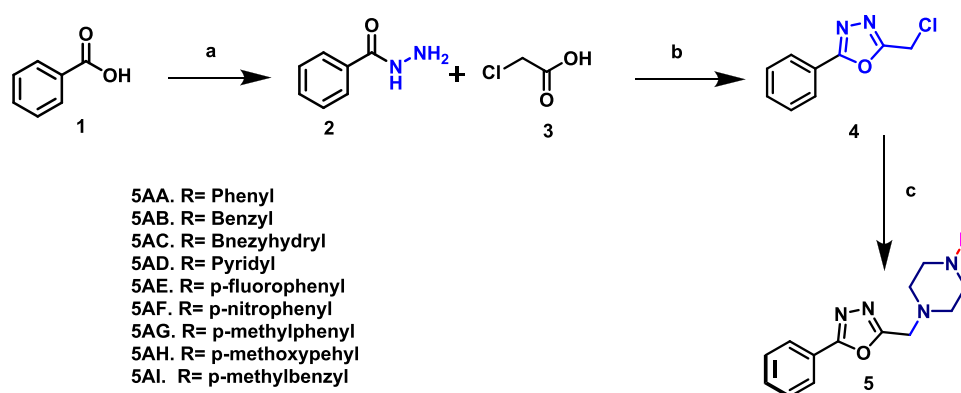


Figure 1. Rationale and designing strategy.

Scheme 1. Synthesis of Target Compounds^a



^aReagents and conditions: (a) HOBT, EDC.HCl, CH₃CN, NH₂NH₂·H₂O, 0–5 °C, 2–3 h, 85–90%, (b) POCl₃, reflux, 2–3 h, 81–86%, and (c) substituted piperazines, K₂CO₃, DMF, rt, 2–3 h, 75–89%.

concomitant inhibition of cholinesterases, BACE-1, Aβ aggregation with better BBB permeability, and antioxidant potential might witness in modifying progression of Alzheimer's disease.¹⁵

In the arduous search of designing novel molecular hybrid, the structural framework of previously reported molecules was utilized namely donepezil comprise of *N*-benzylpiperidine nucleus, which is bound to the catalytic active site (CAS) of AChE. The bioisoteric replacement of piperidine with a piperazine moiety confers the capability of the molecule interacting with the CAS of AChE.^{16,17} Verubecestat, which was a selective BACE-1 under clinical phase trail III, endowed with the 2-pyridyl ring reported for selective binding to aspartate dyad residues responsible for catalytic action.¹⁸ But unfortunately, in clinical trials, rigorous analysis of complete benefit-risk profile has failed.¹⁹ In the recent studies, 1,3,4-oxadiazole and piperazines were found to be the most prescient pharmacophores in the development of new chemical entities due to their excellent role in the designing of drug molecules

against AD.^{20,21} Herein, we have reported oxadiazole tethered with substituted piperazine having phenyl/heterocyclic group possessing varying electron-donating groups (EDGs) and electron-withdrawing groups (EWGs) in order to generate structural activity relationship (SAR).^{22,23} Initially, in silico pharmacophore-based screening approach was utilized to identify hit molecules using Maybridge Database (52,160 compounds).²⁴ Structure-based drug design guided approach inculcating two cocrystals developed for hAChE and hBACE-1, which was deployed to generate in house database. For AChE, one hydrogen bond acceptor, two aromatic ring clusters, and two lipophilic entities were featured, while for BACE-1, two hydrogen bond donors, a positive ionic group, and two aromatic ring clusters were featured in respective e-pharmacophore models. The phase module of Schrodinger Suite 2018 was used to screen an in-house library of 288 compounds. In addition, the generated in-house library of compounds was subjected to virtual screening workflow for extra precision (XP) and standard precision (SP) submodules

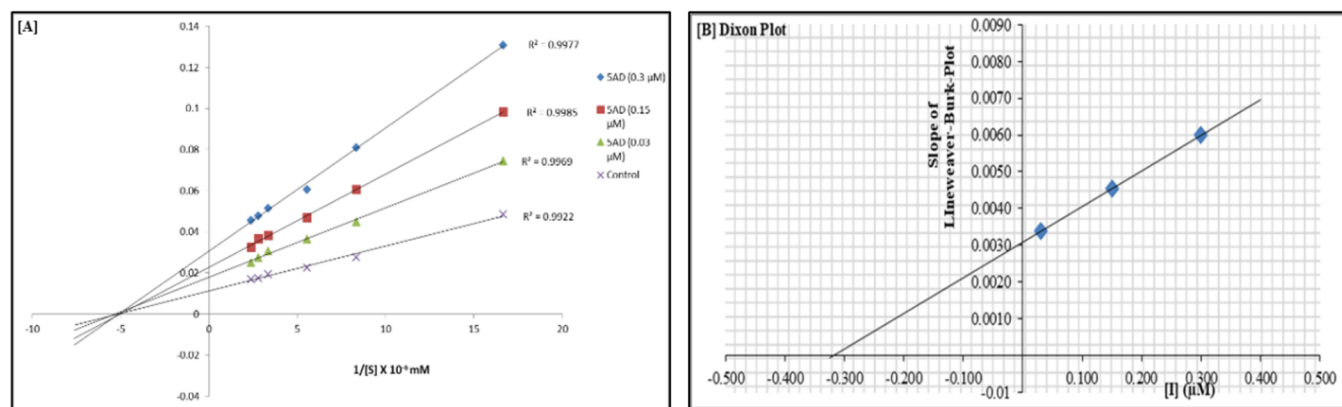


Figure 2. AChE inhibition kinetics of compound **SAD**. (A) Overlaid Lineweaver–Burk reciprocal plot of **SAD** is depicted in the figure. (B) The plot of the slopes against inhibitor concentration for calculation of K_i (Dixon Plot).

with 30% filtration criteria imposed in every step. The screening resulted in 10 compounds, which were further segregated up to 5 on the basis of their docking scores and reflected interactions with their respective catalytic sites (Figure 1). All identified hits were already tested and reported against Alzheimer's targets and were used for further optimizing new molecules against these targets. Taking clues from the extensive literature search, pharmacophore-based designing and molecular hybridization approaches, a series of molecular hybrids of 5-phenyl-1,3,4-oxadiazole linked by methylene and piperazine spacer have been designed, synthesized, and biologically tested against AD. Initially, the compounds were synthesized and further, in vitro evaluation was carried out against multiple targets to check the preliminary efficacy of the molecules, and compounds were found to have potential against hAChE and hBACE-1 in nanomolar ranges. The percentage radical scavenging assay for compound **SAD** was found to be excellent. Furthermore, compounds **SAD**, **SAH**, **SAI**, and **SAB** were subjected to evaluate propidium iodide displacement from PAS of AChE and PAMPA-BBB assay, whereas **SAD** showed the utmost potential among all the tested analogues. In addition, compound **SAD** also exhibited excellent inhibition in self- and AChE-induced aggregation thioflavin T assay. Later, the acute toxicity studies and the Y-maze test were performed in vivo in mice to further substantiate the in vitro findings. The ex vivo investigations on the hippocampal brain tissue homogenate showed that there were notable changes in oxidative stress biomarkers along with decreased AChE levels in a dose-dependent manner.

2. RESULT AND DISCUSSION

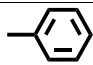
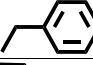
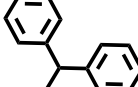
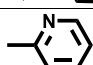
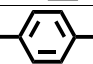
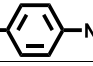

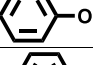
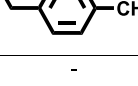
2.1. Chemistry. To synthesize 1,3,4-oxadiazole derivatives, a synthetic route has been optimized, as depicted in Scheme 1. In the first step, benzoic acid was treated with hydrazine hydrate, EDC·HCl, and HOBT with gradual addition of acetonitrile at 0–5 °C followed by continuous stirring of 2–3 h. In addition, phosphorus oxychloride was added gradually to a reaction mixture of benzoic acid hydrazide and 2-chloroacetic acid and refluxed for 3–4 h with continuous stirring to form a precursor to be used for the final step of the synthesis. Eventually, the intermediate was slowly added to piperazine derivatives in the presence of amide coupling reagents HOBT and EDC·HCl at room temperature with continuous stirring for 2 h. The spectroscopic techniques (ATR-FT-IR, ¹H NMR,

and ¹³C NMR) were utilized to characterize the intuitive properties of synthesized conjugates. The spectra of carbohydrazide amines (**2**) displayed stretching band C=N, C=O, and NH in the gamut of 1603–1585, 1665–1632, 3225–3250, cm⁻¹, respectively. The formation of C–Cl bond was confirmed the peak at 640–675 cm⁻¹. The ¹H NMR spectra of compounds (**SAA–SAI**) showed characteristic peak of –CH₂ at δ H = 3.96–3.98 ppm. Similarly, the ¹³C spectra of the compounds (**SAA–SAI**) exhibited the sharp peak in the range δ C = 164.79–159.72 ppm, respectively, to witness the formation of oxadiazole ring.

2.2. In Vitro Biological Assays. **2.2.1. hAChE, hBChE, and hBACE-1 Inhibitory Experiments.** The deficit of brain acetylcholine (AChE) and pertaining transmitters is one of the prominent factors in the aggravation of AD. Clinically, cholinesterase inhibitors are evidence of improving cognitive behavior in AD patients. Thus, Ellman spectroscopic method was utilized to check the multifunctional inhibitory potential of synthesized derivatives against human AChE and BChE and IC₅₀ for all the compounds were reckoned. The compounds **SAA–SAI** showed hAChE inhibition in micromolar range except compound **SAD** (0.103 μM) owing to the substitution of EWGs linked aromatic and heterocyclic rings. Unexpectedly, the replacement with other heterocyclic rings containing electron-withdrawing and electron-releasing groups led to the increase in inhibitory potential up to several folds. The compounds, possessing a *p*-methoxy phenyl substituent, displayed moderate hAChE inhibition (1.477 μM). Further, the substitution with benzyl and *p*-methyl benzyl derivatives rapidly increases the activity against hAChE. All of the synthesized molecules were found to be selective on hAChE except compound **SAI**, which showed more selectivity for BACE-1. There was no such selectivity seen for hBChE.

The study of enzyme kinetics is the determination of the speed at which chemical reactions that enzymes catalyze occur. Thus, it was carried out to investigate the inhibition kinetics for the most potent candidate **SAD** against human AChE. Three separate test compound concentrations were plotted against six different substrate concentrations (acetylthiocholine iodide, ATCI) for generating the Lineweaver–Burk plot. The findings revealed a decrease in V_{max} while the K_m values increased as the inhibitor concentration increased (Figure 2A). The **SAD** has an inhibition rate constant value (K_i) of 0.040 μM deduced after the Dixon plot (Figure 2B).

Table 1. IC₅₀ Values of the Synthesized Compounds

Compounds	R-Group	IC ₅₀ ± SEM (μM) ^a			% RSA of DPPH ± SEM at 25 μM
		hAChE	hBChE	BACE-1	
5AA		1.835 ± 0.076	>10	4.785 ± 0.071	32.20 ± 2.2
5AB		1.786 ± 0.032	>10	>10	42.24 ± 2.5
5AC		3.150 ± 0.0202	>10	5.622 ± 0.073	>10
5AD		0.103 ± 0.0172	>10	1.342 ± 0.078	44.35 ± 2.7
5AE		2.189 ± 0.034	>10	1.485 ± 0.095	31.30 ± 2.4
5AF		1.868 ± 0.0441	>10	6.242 ± 0.030	35.45 ± 2.8
5AG		2.590 ± 0.0169	>10	3.811 ± 0.039	36.30 ± 2.5
5AH		1.477 ± 0.0719	>10	1.685 ± 0.012	38.78 ± 2.9
5AI		1.797 ± 0.0081	>10	0.392 ± 0.021	36.24 ± 2.6
Donepezil	-	0.054 ± 0.006	2.557 ± 0.038	1.413 ± 0.017	39.45 ± 2.8
Rivastigmine	-	1.701 ± 0.024	1.312 ± 0.0013	nd	nd
Ascorbic acid	-	nd	nd	nd	59.65 ± 2.3

^aThe in vitro activity of the synthesized compounds is depicted as IC₅₀ ± SEM of a triplicate experiment (*n* = 3). nd represents the condition of not determining the selectivity and in vitro efficacy.

BACE-1 (β -secretase) is a crucial enzyme engaged in the production of amyloid plaques in Alzheimer's disease. In addition to cholinesterase inhibition, the hBACE-1 inhibitory potency for the aforementioned series of compounds was evaluated. Insoluble fragments of Amyloid- β are formed by catalytic proteolysis of amyloid precursor protein (APP) with the help of the BACE-1 enzyme. BACE-1 inhibition endowed supreme potency in addition to similar AChE activity with the substituent having *p*-methyl benzyl (compound **5AI**, 0.392 μ M). Other tested compounds bearing *p*-methoxy benzyl (1.685 μ M), pyridyl, and *p*-fluorophenyl exhibited moderate inhibition in micromolar ranges. Some of them displayed lower inhibition against BACE-1 signifying that the substituents are showing little activity against the target (Table 1).

2.2.2. DPPH Radical Scavenging Assay. DPPH (2,2-diphenyl-1-picrylhydrazyl) free radical scavenging assay was carried out for the synthesized oxadiazole-piperazine conjugates using different concentrations in methanol using ascorbic acid as a positive test control, and the decrease in absorbance was monitored by a visible spectrophotometer at 517 nm. Initially, the color of the reaction mixture was purple and turned yellow in the presence of inhibitor. The results are summarized in Table 1. Compound **5AD** (44.35%) and **5AB** (42.24%) exhibited a maximum percentage of radical

scavenging activity compared to other derivatives and similar activity to that of positive control ascorbic acid. Other derivatives also shown optimum antioxidant potential. The activity of these conjugates may be due to the quaternized form of piperazine -NH in a biological environment, which provides hydrogen to the DPPH.

2.2.3. Thioflavin-T-Based A β Aggregation Assay. The brain permeability assay suggested considerable permeability along with propidium iodide displacement potential at PAS-AChE. It has been found that cholinesterase inhibitors bound to the peripheral active site (PAS) not only result in AChE inhibition but also fend off A β ₁₋₄₂ production and deposition. Therefore, the thioflavin T-based fluorometric assay was carried out for compound **5AD** to reveal PAS binding to AChE and prevent A β ₁₋₄₂ aggregation and deposition. In particular, three different concentration ratios of A β vs inhibitor (10:5, 10:10, 10:20 μ M) for self- and AChE-induced A β ₁₋₄₂ aggregation inhibition were carried out. Normalized fluorescence intensity (NFI) and percentage A β ₁₋₄₂ aggregation parameters were used to assess the A β ₁₋₄₂ aggregation activity. The culmination was observed with a 20 μ M inhibitor concentration. The results implied that there is a concentration-dependent A β ₁₋₄₂ aggregation inhibition by compound

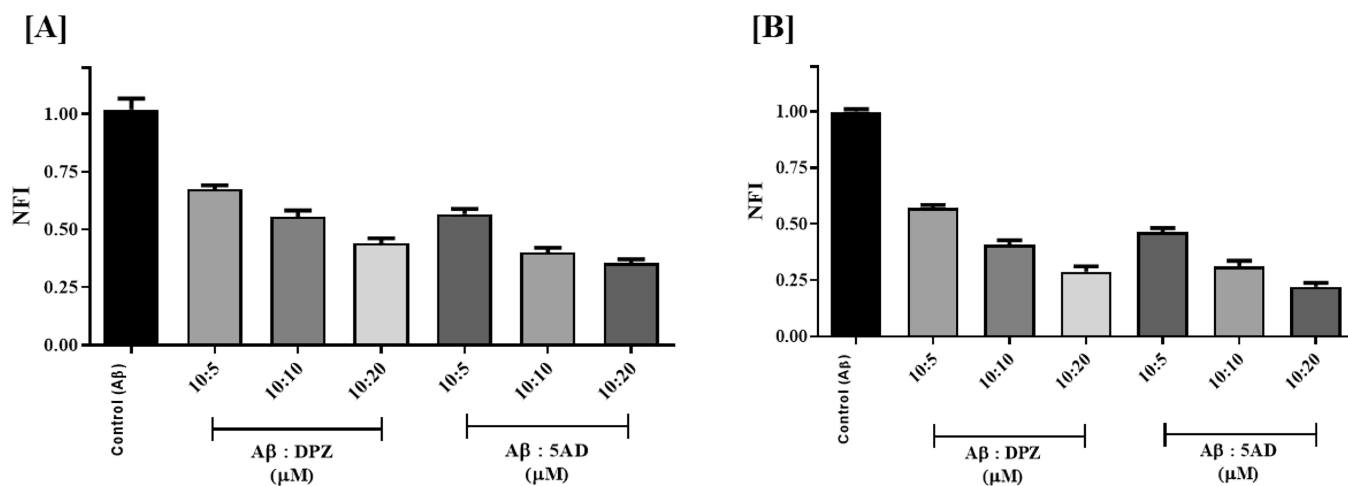


Figure 3. (A) Inhibition of Aβ₁₋₄₂ self-induced aggregation. (B) AChE-induced Aβ₁₋₄₀ aggregation by SAD and the reference compound donepezil (DPZ). The data represent the mean ± SEM of three independent experiments.

Table 2. PAS-AChE Binding Efficiency from the Propidium Iodide and PAMPA-BBB Permeability Assay

compounds	(% PAS-AChE propidium iodide displacement (inhibition) ^a)		PAMPA-BBB permeability*	
	at 10 μM	at 50 μM	$P_{e(\text{exp})}$ (4.8×10^{-6} cm s ⁻¹)	prediction
SAH	19.2 ± 1.812	26.7 ± 1.345	5.8 ± 0.175	CNS ^{+b}
SAD	24.5 ± 1.425	30.4 ± 1.067	6.5 ± 0.072	CNS ^{+b}
SAI	17.7 ± 1.264	28.4 ± 1.415	5.5 ± 0.250	CNS ^{+b}
SAB	18.4 ± 1.069	29.5 ± 1.331	4.8 ± 0.162	CNS ^{+b}
donepezil	23.1 ± 1.025	34.2 ± 1.228	6.8 ± 0.061	CNS ^{+b}

^aData are expressed as the mean ± SEM of three separate experiments ($n = 3$). ^bCNS⁺ compounds with value $P_e > 4.8 \times 10^{-6}$ cm s⁻¹ showing excellent BBB permeability.

SAD and PAS-AChE inhibition, which may be a key factor in Aβ₁₋₄₂ aggregation inhibition and deposition (Figure 3).

2.2.4. Blood–Brain Barrier (BBB) Permeability Assay. The parallel artificial membrane permeability assay (PAMPA) is used as an in vitro model of passive and transcellular permeation. PAMPA avoids the complexities of active transport, allowing test compounds to be ranked based on a simple permeability property alone. The brain permeability of the compounds targeting CNS requires to be tested. The PAMPA assay was carried out using the reported method by Di et al.²⁵ and experimental results ($P_{e(\text{exp})}$) were compared with the previously recorded results ($P_{e(\text{ref})}$) of nine marketed drugs and measured the gamut of permeability values for excellent, uncertain, and poor permeability values as per our previously reported procedures. PAMPA-BBB assay results are displayed in Table 2. The tested compounds SAI, SAH, and SAB showed peculiar permeability values, whereas compound SAD has a significantly comparable value for the permeability as compared to donepezil.

2.2.5. PAS-AChE Binding Efficiency Assay. Propidium iodide displacement assay was performed for the potential scaffolds using the procedure reported by Taylor et al.²⁶ in order to validate our hypothesis that the developed ligand will bind with PAS-AChE. A well-known ligand, propidium iodide, has been shown to bind to PAS-AChE specifically and to boost the fluorescence intensity by up to 8–10 times. The decrease intensity recorded due to the PI displacement from PAS-AChE in the presence of the inhibitor at 10 and 50 μM (Table 2). The observed results indicated lower propidium iodide displacement capability by compounds SAH, SAB, and SAI,

while compound SAD displayed significantly higher displacement than propidium iodide, in contrast to donepezil at 10 and 50 μM concentrations. The outcome of the propidium iodide displacement assay exhibited an inherent binding capability of compound SAD at PAS-AChE (Table 2).

The outcomes suggested that compound SAD displayed significant inhibition for AChE, BChE, and BACE-1. Compound SAD has also predicted considerable results in the case of propidium iodide displacement assay and BBB permeability studies. Therefore, compound SAD was selected as a lead molecule for forthcoming pharmacological studies.

2.3. In Vivo Biological Experiments. **2.3.1. Acute Toxicity Observations.** Using healthy Swiss albino mice, the acute toxicity tests were carried out in line with OECD procedure 423. As per the guidelines, 14 days of toxicity testing protocol were followed for SAD, where it was well tolerated and did not exhibit any toxicity or aberrant reactions at the highest dose of 100 mg/kg, p.o. The result implies a substantial degree of safety and could be further tested in vivo in mice.

2.3.2. Short-Term Memory Impairment Test using Scopolamine Y-Maze Model. The in vivo efficacy of compound SAD for improving memory and learning was evaluated using the Y-maze test in Swiss Albino mice where scopolamine was used as an inducing agent. Scopolamine is frequently employed to induce cognitive impairment resulting from a deficiency in cholinergic activity. The Y-maze test is a widely used animal model in memory research. It evaluates the acquired behaviors of animals by measuring their spontaneous alteration score.²⁷ The mice treated with a dosage of 1 mg/kg of compound SAD showed a notable improvement in alterations compared with

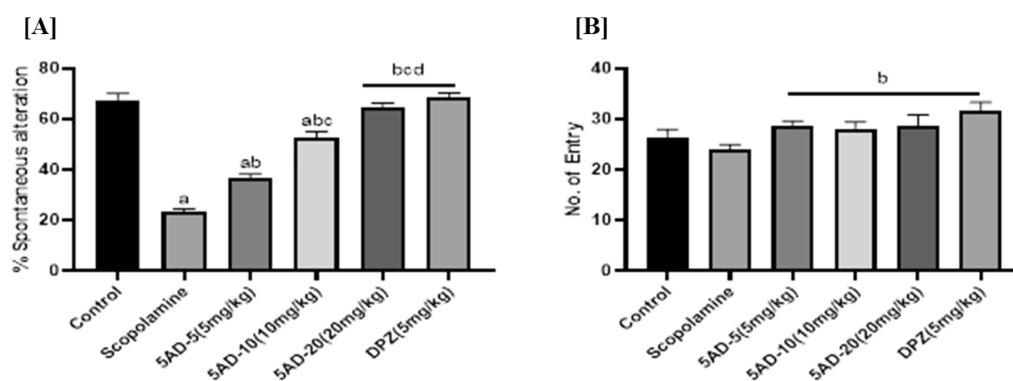


Figure 4. Y-maze test: effect of **5AD** on mice ($n = 6$) was individually placed into a symmetrical Y-maze. (A) % Spontaneous alteration. (B) Total number of arm entries. Dunnett's multiple comparison test calculated data presented as mean \pm SEM and p -values; ^a $p < 0.05$, ^{ab} $p < 0.01$, ^{abc} $p < 0.001$, ^{abcd} $p < 0.0001$.

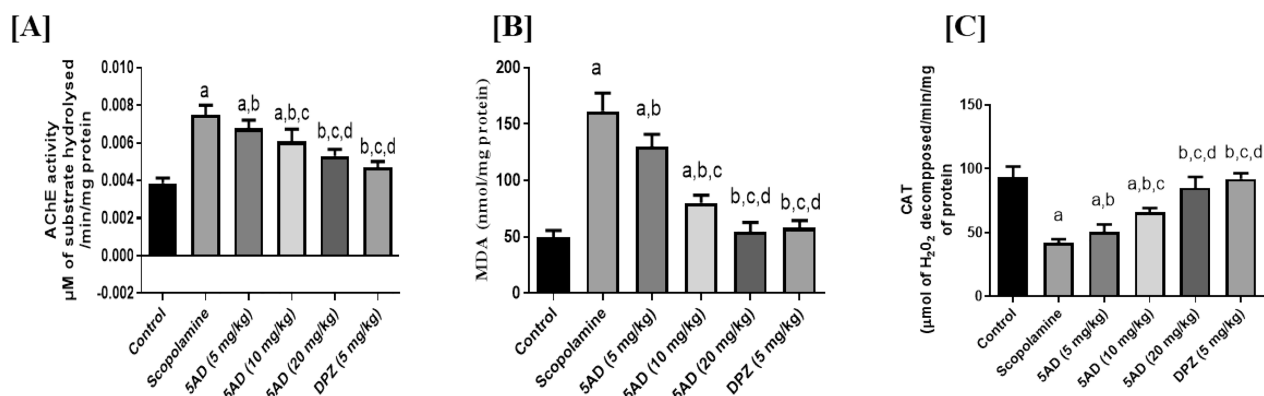


Figure 5. Neurochemical estimation of compound **5AD** in the prepared brain homogenates; (A) level of AChE; (B) MDA level observation in TBARS assay; (C) CAT level estimation. All the estimated values are depicted as the mean \pm SEM ($n = 6$); ^a $p < 0.05$, ^{ab} $p < 0.01$, ^{abc} $p < 0.001$, ^{abcd} $p < 0.0001$.

the groups treated with scopolamine. However, this improvement was not statistically significant when compared to the control group. Compound **5AD** was found to be less potent as compared to the standard drug donepezil at the similar dose, but a considerable boom up in spontaneous alteration score (Figure 4A) at a dose of 5 mg/kg compared to donepezil of 1 mg/kg dose probably seems to be because of combined AChE and BACE-1 inhibitory potential.²⁸ The animals were acclimated, and their aura of producing fear and anxiety of new environments were assessed by counting their novel arm entries (Figure 4B). The administration of compound **5AD** resulted in a reduction in anxiety and cainophobia behaviors in mice in comparison to the effects produced with scopolamine.

2.4. Ex Vivo Experiments and Neurochemical Estimation. **2.4.1. AChE Level Determination.** The impact of compound **5AD** on the acetylcholinesterase level using extracted homogenates from the hippocampus part of brain was estimated by using reported protocol by Ellman's with little modification. The findings indicated that the levels of AChE were notably elevated in the groups treated with donepezil and compound **5AD**, in comparison with the group treated with scopolamine (Figure 5A). The studies also demonstrated the capacity of compound **5AD** to penetrate the blood–brain barrier (BBB).²⁹

2.4.2. Determination of ROS Induced Oxidative Stress Biomarkers. The free radical produced in the body was nullified by body defense mechanisms via several antioxidants present in healthy conditions of our body. An excessive

perturbation in this mechanism resulted in massive free radical generation, and if untreated, it is lethal to the neuronal cells and threatening to cognitive behavior. In such prevailing conditions, artificial or chemically synthesized antioxidants are a prerequisite to delay or prevent the detrimental effects by quenching them. Biochemical evaluation of many oxidative indicators at the required tested dose for memory and learning impairment (5 mg/kg) was done in order to explore the antioxidant influence of our compound **5AD**.

The generated reactive species possess a profound affinity toward lipids. Polyunsaturated lipids are plentiful in the brain region, and oxidative damage and lipid peroxidation are major risks associated with elevated lipid concentrations. Malonaldehyde (MDA) was estimated using the reactive components of thiobarbituric acid (TBA), which is one of the final products of LPO. In the scopolamine-treated group, the MDA/mg protein level was considerably greater than that in the control group, suggesting a higher degree of oxidative stress. Compound **5AD**'s antioxidant capacity was supported by the fact that its treatment group showed a lower level of MDA than the scopolamine-treated group. In contrast, the donepezil-treated (control) batch showed negligible MDA levels when compared to the scopolamine-treated group (Figure 5B).³⁰

Hydrogen peroxide, a nonradical ROS, is the substrate for the essential enzyme catalase. In order to keep an optimum level of the molecule in the cell, which is also necessary for cellular signaling activities, this enzyme neutralizes hydrogen peroxide through its breakdown. There was significant

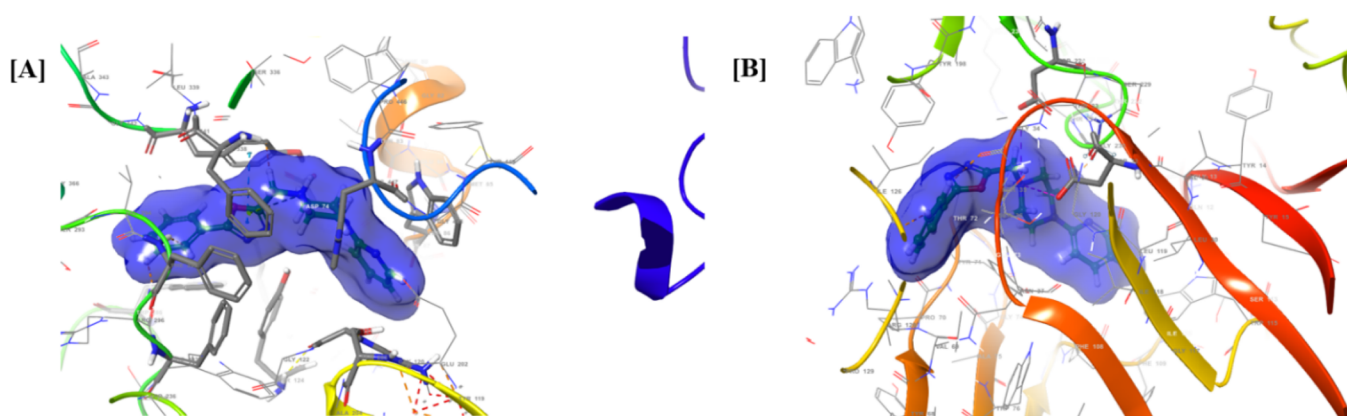


Figure 6. Docked poses displaying interaction of compound **5AD** in the site of (A) hAChE (PDB ID: 4EY7): The PAS residues are depicted as blue (Asp74, Tyr124, Tyr72, and Trp286), anionic subsite (Trp86, Glu202, and Phe338), ABP (Phe295 and Phe297), CAS (Ser203, His447, and Glu334), and OAH (Gly120, Gly121, and Ala204). (B) hBACE-1 (PDB ID: 2ZJM). Docking involves Aspartate dyad residues' interaction with Asp32 and Asp228 in bold lines.

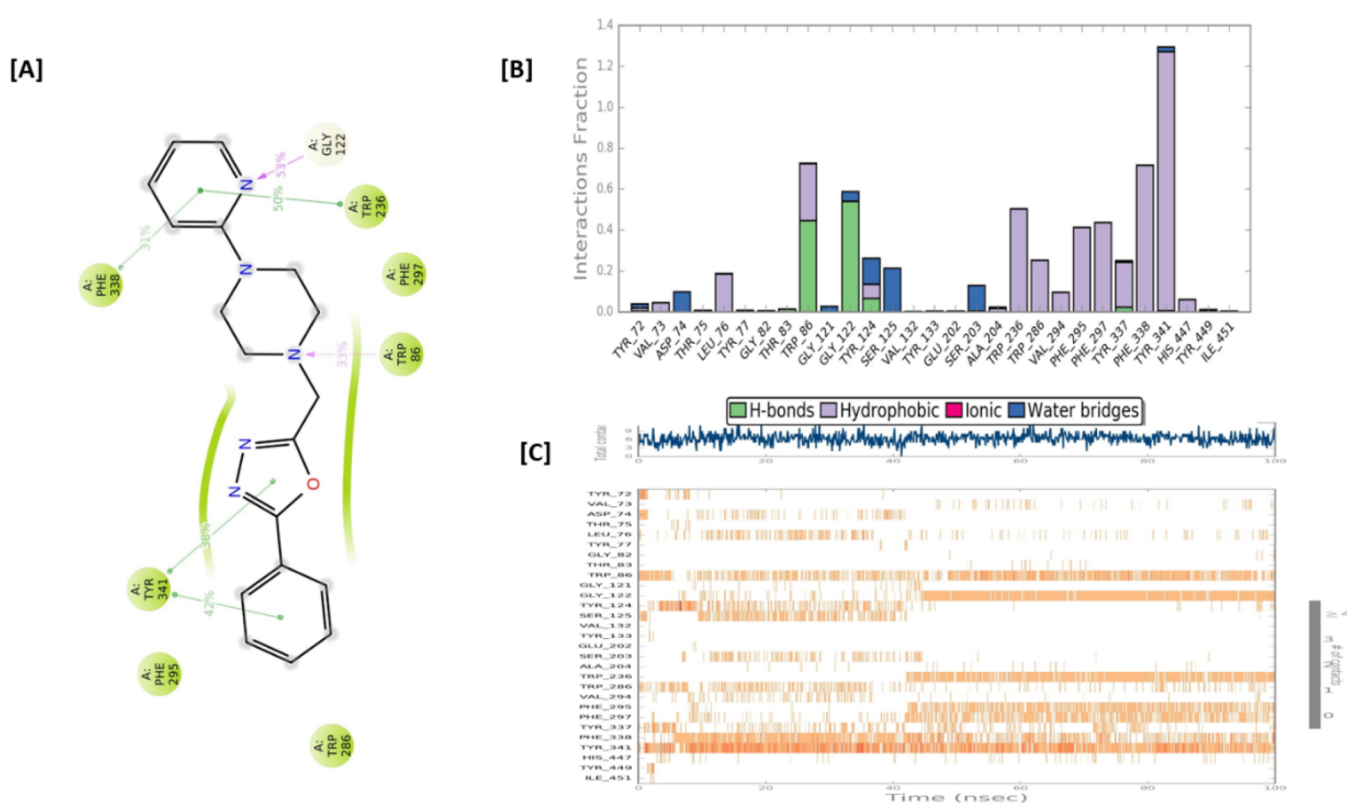


Figure 7. Dynamics studies of docked complexes of compound **5AD** with hAChE; (A) percent stability of interactions; (B) histogram displaying amino acid interaction fractions; (C) time-intensive interaction of each amino acid up to 100 ns.

amelioration observed in the catalase activity in the prepared brain homogenate in the different treated groups (Figure 5C). The ex vivo assessment of oxidative stress biomarkers indicates that compound **5AD**, administered at a dose of mg/kg, exhibited a similar antioxidant capacity compared with the groups treated with the standard drug donepezil. Hence, compound **5AD** was found to be a potential compound for counteracting oxidative stress induced by scopolamine along with improved learning memory.

2.5. In Silico Experiments. 2.5.1. Molecular Docking Analysis and MM-GBSA. Docking studies were performed to gain in-depth interaction of compound **5AD** with the active site residues of the acetylcholinesterase and β -secretase-1 using

the Schrodinger Glide module. The protein grid that was generated in the beginning and was confirmed by isolating and cocrystallized ligand (donepezil) redocking, namely, FIM for hBACE-1 (PDB ID: 2ZJM) and donepezil (DNP) for hAChE (PDB ID: 4EY7). The superposition tool was employed to calculate the root-mean-square deviation (RMSD) values between the docked and cocrystallized conformations of ligands. This analysis was conducted within a 1.9 Å limit to verify the accuracy of the produced grids and the established protocols for docking. The compound **5AD** underwent docking using the Schrodinger's Glide XP module, and XP visualizer tool was used for displaying the results. The relative energy for docked complex was calculated by using the Prime-

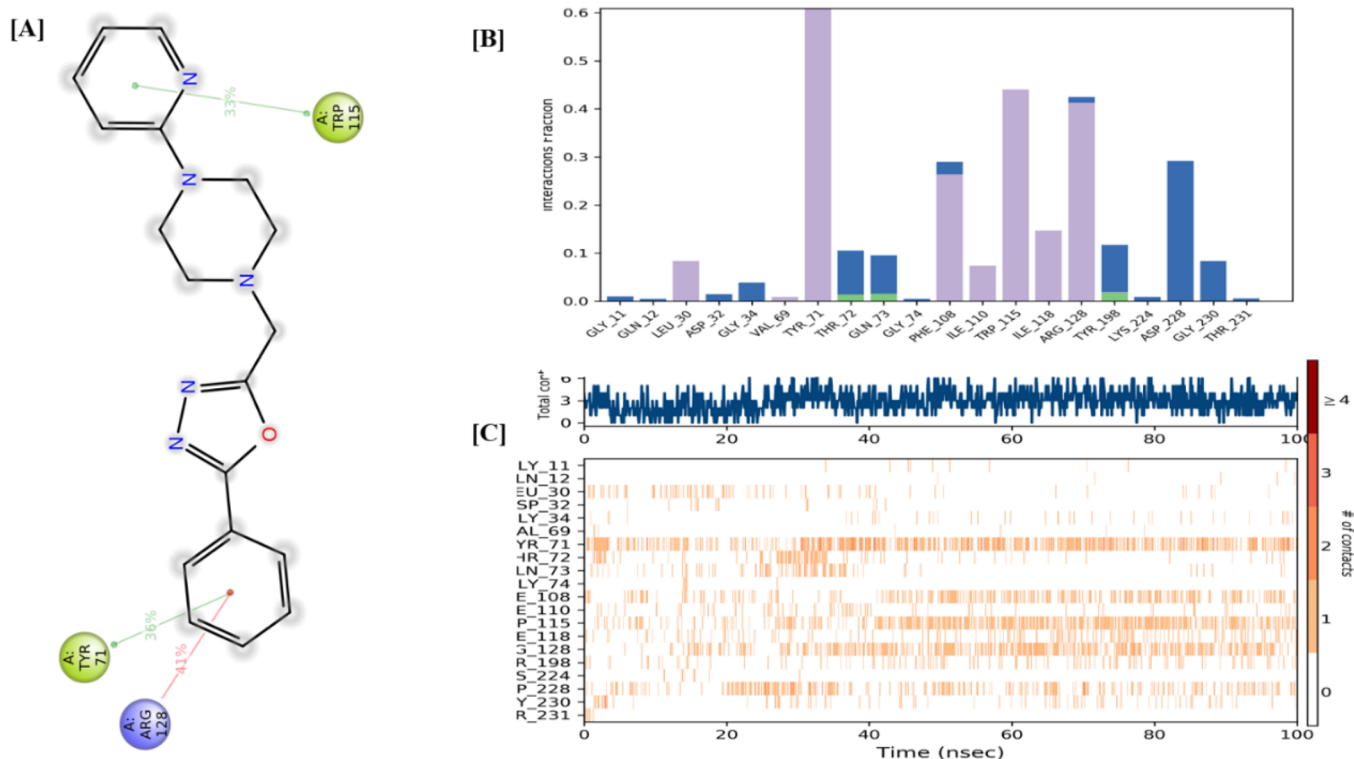


Figure 8. Dynamics studies of docked complexes of compound **SAD** with hBACE-1; (A) percent stability of interactions; (B) histogram displaying amino acid interaction fractions; (C) time-intensive interaction of each amino acid up to 100 ns.

MMGBSA tool, and relative energy for compound **SAD** was found to be -61.547 kcal/mol for AChE and -58.523 for BACE-1 (Figure S23, Supporting Information).

The docking investigations on hAChE revealed that compound **SAD** had a confirmed proximity into the extrapolated deep cavity of CAS and PAS residues. The oxadiazole nucleus exhibited electrostatic contacts with Asp74 and head-to-head interactions with Tyr341 at the PAS domain. Additionally, the Trp286 and Tyr124 amino acids of the PAS site showed hydrophobic interactions with the tilted 2-pyridyl piperazine moiety in **SAD** (Figure 6A). Furthermore, compound **SAD** exhibited its binding mode capability on hBACE-1 (PDB ID: 2ZJM), as depicted in the figure. The docking studies on hBACE-1 revealed that compound **SAD** demonstrated an established contact with the catalytic dyad residues (Asp32 and Asp228). The N atom of the piperazine nucleus establishes interaction with Asp32 and Asp228 via building of a salt bridge (Figure 6B).

2.5.2. Simulation Studies. The dynamics phase run for 100 ns was performed to confirm the stability of docked complexes of compound **SAD** against hBACE-1 and hAChE (Figure 7). The RMSD values were calculated for consolidated 100 ns run to assess the protein–ligand interaction stability with respect to the backbone structure of the selected proteins. The outcomes indicated that the RMSD for the docked complexes was observed within the standard limit of 1–3 Å. The ligand–protein interaction was visualized using histograms, timeline, and 2D graphics representations. (Figure 8).

2.5.3. In Silico ADME Prediction and Cell Line Toxicity Studies. The ADME prediction of compound **SAD** was carried out to check the physicochemical and chemical properties associated with the molecule (Figure S22, Supporting Information). Compound **SAD** was qualifying the Lipinski

rule of 5, that is, molecular weight of the compound **SAD** is 321.38 less than 500, and numbers of H-bond acceptors are equal to 5 with no H-bond donors. The $\text{Log } P_0/w$ (iLogP) and total polar surface area of the compound were found to be 3.2 and 58.29 Å, which revealed that compound **SAD** has good oral and intestinal absorption while TPSA implied excellent BBB permeability, which was also indicated in the pharmacokinetics prediction.³¹ A Way2Drug cytotoxic cell line prediction was performed to check the toxicity of compound **SAD** where it showed P values less than 0.5 indicating devoid of cell line toxicities.³²

3. CONCLUSIONS

It is fact that numerous pathogenic pathways govern the progression of Alzheimer's disease (AD) and, therefore, researchers are now emphasizing on designing of candidates to target different pathogenic pathways simultaneously. Herein, multisubstituted hybrid molecules of 5-phenyl-1,3,4-oxadiazoles with pyridylpiperazine linked with a methylene spacer was designed and evaluated their potency against major AD targets, namely, hAChE, hBChE, hBACE-1, and $A\beta$. In particular, compound **SAA-5A1** displayed balanced and significant inhibition in the range of nanomolar to micromolar ranges against both targets concurrently. The BBB permeability of screened inhibitors was assessed using the PAMPA-BBB assay, and their capacity to displace propidium iodide was evaluated using the PAS-AChE displacement assay. The result suggested that compound **SAD** has significant potential to penetrate the BBB and to displace propidium iodide from the peripheral active site in contrast to donepezil. Based on permeability and PAS-AChE assay results, compound **SAD** was evaluated for their $A\beta$ aggregation inhibition using thioflavin T assay and results demonstrated dose-dependent reduction compared to

donepezil. Further, in vivo acute toxicity was checked and 100 mg/kg dose was found to be significant, maximally and at the same time, behavioral test for learning spatial memory implied that compound **SAD** has significantly ameliorating effect of scopolamine. Furthermore, the analysis of mice brain homogenate using ex vivo and neurochemical methods revealed a notable suppression of AChE and demonstrated the antioxidant capabilities of compound **SAD** and results were substantiated by molecular dynamics and molecular simulation studies. The overall studies against the AD revealed that compound **SAD** could further be optimized, and it can be a potential lead molecule.

4. MATERIALS AND METHODOLOGY

4.1. Chemistry. 4.1.1. Chemicals and Instrumentation.

All the prerequisite standard quality chemicals with 99% purity were purchased and procured from several certified commercial sources such as TCI Chemicals (Chennai, India), Avra Synthesis (Hyderabad, India), and Sigma-Aldrich (Bengaluru, India), and used without further purification for the synthesis of several derivatives. TLC silica gel G60 aluminum sheets (Merck, India) were used, and R_f values were determined using UV light ($\lambda = 254$ nm), Dragendorff reagent, or iodine vapors. The melting points for the synthesized sample were reckoned on the MP55 melting point system (Mettler Toledo, Mumbai, India) using two slip melting point capillaries. Mass spectra were recorded on a 6410 Triple Quadrupole LC/MS (Agilent, USA) in positive ion mode using an electrospray ionization (ESI) source.

FT-IR spectra were acquired from an Alpha ECO-ATR spectrophotometer (Bruker, USA). NMR spectra (^1H NMR: 500 MHz and ^{13}C NMR: 125 MHz) were recorded on a Bruker Avance FT-NMR spectrophotometer (Bruker, USA), and chemical shift values (δ) were reported as ppm standard to tetramethylsilane (TMS) using $\text{DMSO-}d_6$ and CDCl_3 as solvents. Further, the spectra were analyzed using MetReNova 6.0.2 software tool.

4.1.2. Synthesis of Benzoic Acid Hydrazide 2. Benzoic acid (1, 8.188 mmol), HOBT (9.76 mmol), and EDC. HCl (9.80 mmol) were added to acetonitrile at 0–5 °C followed by continuous stirring to form a clear solution. To this mixture was gradually added dropwise with hydrazine hydrate (16.35 mmol) with continuous stirring at room temperature for 2–3 h. The reaction mixture was proctored using TLC (EA:hexane, 50:50 v/v), and solvents were evaporated using a rotary evaporator. The crude product was precipitated using hexane and ethyl acetate (3:9 ratio) followed by drying to form pure compound **2**.³³

4.1.3. Procedure for Synthesis of Compound 4. A mixture of intermediate **2** and 2-chloroacetic acid, phosphorus oxychloride, and a dehydrating agent was added dropwise in a fuming cupboard with continuous stirring for 2–3 min. Further, the resultant mixture was refluxed for 2–3 h continuously and reaction completion was monitored using TLC (EA:hexane, 50:50 v/v). After completion of the reaction, it was allowed to cool at room temperature followed by subsequent addition of 5% sodium bicarbonate (NaHCO_3) solution with continuous agitation until a precipitate gets formed. The precipitate was then collected and dried over Na_2SO_4 .³⁴

4.1.4. Synthetic Protocol for Screened Inhibitors. The coupled intermediate **4** underwent a nucleophilic substitution reaction to form final compounds. Initially, substituted

piperazines were added gradually in a 50 mL round-bottomed flask containing 5 mL of DMF, followed by the addition of potassium carbonate (K_2CO_3), with continuous stirring using a magnetic stirrer for a few minutes. Then, intermediate **4** was added gradually to the solution with continuous stirring for 2–3 h at room temperature, and the reaction progress was monitored by using TLC.

4.1.4.1. 2-Phenyl-5-((4-phenylpiperazin-1-yl)methyl)-1,3,4-oxadiazole (5AA). Yield: 75%; off-white solid; mp; 176–178 °C; TLC (hexane:EA, 50:50 v/v); $R_f = 0.66$. FT-IR (Alpha ATR, ν cm^{-1}): 1693 (C=N); 1340 (C–N aromatic); 1676 (C–C aromatic). ^1H NMR (500 MHz, DMSO) δ 8.03 (s, 2H), 7.64 (s, 3H), 7.22 (s, 2H), 6.92 (s, 2H), 6.76 (s, 1H), 3.93 (s, 2H), 3.18–3.15 (m, 4H), 2.68 (s, 4H). ^{13}C NMR (12 MHz, DMSO) δ : 165.42, 163.93, 150.44, 132.63, 131.43, 129.71, 126.87, 123.67, 119.35, 116.22, 100.10, 51.79, 51.19, 49.48, 18.38. HRMS $[\text{M} + 1]^+$ calcd 335.1866, found 335.1827

4.1.4.2. 2-((4-Benzylpiperazin-1-yl)methyl)-5-phenyl-1,3,4-oxadiazole (5AB). Yield: 68%; off-white solid; mp; 196–198 °C; TLC (hexane:EA, 50:50 v/v); $R_f = 0.68$. FT-IR (Alpha ATR, ν cm^{-1}): 1695 (C=N); 1355 (C–N aromatic); 1678 (C–C aromatic). ^1H NMR (500 MHz, DMSO) δ : 7.99 (s, 2H), 7.61 (s, 3H), 7.27 (s, 5H), 3.89 (s, 2H), 3.45 (s, 2H), 2.54 (s, 4H), 2.40 (s, 4H). ^{13}C NMR (125 MHz, DMSO) δ : 164.77, 163.84, 138.60, 132.38, 129.94, 129.21, 128.62, 127.42, 127.03, 123.84, 62.43, 60.44, 52.88, 50.89, 21.00, 14.96. HRMS $[\text{M} + 1]^+$ calcd 335.2050, found 335.1827.

4.1.4.3. 2-((4-Benzhydrylpiperazin-1-yl)methyl)-5-phenyl-1,3,4-oxadiazole (5AC). Yield: 68%; off-white solid; mp; 196–198 °C; TLC (hexane:EA, 50:50 v/v); $R_f = 0.68$. FT-IR (Alpha ATR, ν cm^{-1}): 1695 (C=N); 1355 (C–N aromatic); 1678 (C–C aromatic). ^1H NMR (500 MHz, DMSO) δ 8.00 (d, $J = 6.6$ Hz, 2H), 7.62 (dt, $J = 14.1, 6.9$ Hz, 3H), 7.44–7.37 (m, 4H), 7.28 (t, $J = 7.6$ Hz, 4H), 7.17 (t, $J = 6.7$ Hz, 2H), 4.27 (s, 1H), 3.89 (s, 2H), 2.57 (s, 4H), 2.34 (s, 4H). ^{13}C NMR (125 MHz, DMSO) δ : 164.97, 164.00, 143.42, 132.67, 129.94, 128.98, 128.02, 127.31, 127.04, 123.83, 75.65, 52.68, 51.83, 51.43, 40.25. HRMS $[\text{M} + 1]^+$ calcd 411.2178, found 411.2140.

4.1.4.4. 2-Phenyl-5-((4-(pyridin-2-yl)piperazin-1-yl)methyl)-1,3,4-oxadiazole (5AD). Yield: 89%; crystalline white solid; mp; 192–194 °C; TLC (hexane:EA, 50:50 v/v); $R_f = 0.59$. FT-IR (Alpha ATR, ν cm^{-1}): 1626 (C=N); 1341 (C–N aromatic); 1677 (C–C aromatic). ^1H NMR (500 MHz, DMSO) δ 8.10 (d, $J = 4.9$ Hz, 1H), 8.02 (d, $J = 7.9$ Hz, 2H), 7.63 (dd, $J = 10.7, 7.1$ Hz, 3H), 7.52 (t, $J = 7.8$ Hz, 1H), 6.82 (d, $J = 8.6$ Hz, 1H), 6.66–6.60 (m, 1H), 3.96 (s, 2H), 3.59–3.42 (m, 4H), 2.75–2.56 (m, 4H). ^{13}C NMR (125 MHz, DMSO) δ : 164.88, 164.13, 159.69, 148.13, 138.01, 132.60, 130.27, 126.99, 124.13, 113.59, 107.69, 52.39, 51.68, 44.86, 39.93. HRMS $[\text{M} + 1]^+$ calcd. 322.1728, found 322.1623

4.1.4.5. 4-((4-Fluorophenyl)piperazin-1-yl)methyl)-5-phenyl-1,3,4-oxadiazole (5AE). Yield: 85%; white solid; mp; 152–154 °C; TLC (hexane:EA, 50:50 v/v); $R_f = 0.55$. FT-IR (Alpha ATR, ν cm^{-1}): 1677 (C=N); 1393 (C–N aromatic); 1647 (C–C linked to piperazine), 1393 (C–F, aromatic). ^1H NMR (500 MHz, DMSO) δ 8.02 (d, $J = 6.5$ Hz, 2H), 7.68–7.58 (m, 3H), 7.04 (t, $J = 8.9$ Hz, 2H), 6.94 (dd, $J = 9.2, 4.7$ Hz, 2H), 3.97 (s, 2H), 3.36 (s, 15H), 3.10 (s, 4H), 2.69 (s, 4H), 2.51 (s, 2H). ^{13}C NMR (500 MHz, DMSO) δ 214.41, 195.85, 164.88, 164.08, 157.69, 155.58, 148.25, 132.79, 129.88, 127.18, 123.87, 118.08, 115.80, 52.81, 51.42, 49.32, 40.23; HRMS $[\text{M} + 1]^+$ calcd 339.1621, found 339.1576.

4.1.4.6. 2-((4-(4-Nitrophenyl)piperazin-1-yl)methyl)-5-phenyl-1,3,4-oxadiazole (**5AF**). Yield: 78%; yellow solid; mp; 186–188 °C; TLC (hexane:EA, 50:50 v/v); R_f = 0.6. FT-IR (Alpha ATR, ν cm^{-1}): 1692 (C=N); 1386 (C–N aromatic); 1677 (C–C aromatic). ^1H NMR (500 MHz, DMSO) δ 8.03 (dd, J = 20.2, 8.5 Hz, 4H), 7.72–7.55 (m, 3H), 7.03 (d, J = 9.5 Hz, 2H), 3.99 (s, 2H), 3.50 (s, 4H), 2.69 (s, 4H). ^{13}C NMR (125 MHz, DMSO) δ : 165.05, 164.24, 155.39, 137.63, 132.59, 129.94, 127.37, 126.14, 123.92, 113.43, 52.14, 51.36, 46.71, 40.31. HRMS $[\text{M} + 1]^+$ calcd 366.1831, found 366.1521.

4.1.4.7. 2-Phenyl-5-((4-(*p*-tolyl)piperazin-1-yl)methyl)-1,3,4-oxadiazole (**5AG**). Yield: 84%; white solid; mp; 156–158 °C; TLC (hexane:EA, 50:50 v/v); R_f = 0.68. FT-IR (Alpha ATR, ν cm^{-1}): 1696 (C=N); 1391 (C–N aromatic); 1642 (C–C linked to piperazine). ^1H NMR (500 MHz, DMSO) δ 8.03 (s, 2H), 7.63 (s, 3H), 7.02 (s, 2H), 6.84 (s, 2H), 3.96 (s, 2H), 3.10 (s, 4H), 2.69 (s, 4H), 2.19 (s, 3H). ^{13}C NMR (125 MHz, DMSO) δ : 165.02, 164.11, 149.26, 132.37, 129.67, 128.35, 126.73, 123.84, 116.39, 52.69, 51.34, 49.12, 39.84, 20.51. HRMS $[\text{M} + 1]^+$ calcd 335.1866, found 335.1827.

4.1.4.8. 2-((4-(4-Methoxyphenyl)piperazin-1-yl)methyl)-5-phenyl-1,3,4-oxadiazole (**5AH**). Yield: 86%; white solid; mp; 188–190 °C; TLC (hexane:EA, 50:50 v/v); R_f = 0.72. FT-IR (Alpha ATR, ν cm^{-1}): 1693 (C=N); 1391 (C–N aromatic); 1250 (C–O aromatic). ^1H NMR (500 MHz, CDCl_3) δ 8.11 (s, 5H), 7.55 (s, 8H), 6.93 (s, 5H), 6.87 (s, 5H), 3.99 (s, 5H), 3.17 (s, 10H), 2.84 (s, 10H), 1.63 (s, 9H). ^{13}C NMR (125 MHz, CDCl_3) δ : 165.45, 163.49, 154.14, 145.38, 131.75, 129.42, 126.88, 124.17, 118.56, 114.47, 76.77, 55.67, 53.18, 52.23, 50.63. HRMS $[\text{M} + 1]^+$ calcd 351.1829, found 351.1776.

4.1.4.9. 2-((4-(4-Methylbenzyl)piperazin-1-yl)methyl)-5-phenyl-1,3,4-oxadiazole (**5AI**). Yield: 81%; white solid; mp; 145–147 °C; TLC (hexane:EA, 50:50 v/v); R_f = 0.72. FT-IR (Alpha ATR, ν cm^{-1}): 1693 (C=N); 1395 (C–N aromatic); 1677 (C–C aromatic). ^1H NMR (500 MHz, DMSO) δ 8.01 (d, J = 10.3 Hz, 2H), 7.62 (d, J = 9.9 Hz, 3H), 7.15 (s, 2H), 7.12 (s, 2H), 3.88 (s, 2H), 3.40 (s, 2H), 2.51 (d, J = 1.2 Hz, 4H), 2.37 (s, 4H), 2.27 (s, 3H). ^{13}C NMR (500 MHz, DMSO) δ : 164.90, 164.24, 136.47, 135.56, 132.48, 129.94, 129.27, 129.18, 127.03, 123.88, 62.28, 52.89, 52.72, 51.56, 21.26. HRMS $[\text{M} + 1]^+$ calcd 349.2199, found 349.1984.

4.2. In Vitro Cholinesterase Inhibition Assay (hAChE and hBChE). The Ellman's colorimetric technique was used to assess cholinesterase inhibition of the synthesized scaffolds in accordance with the published protocol.³⁵ To create human acetylcholinesterase from people, RBC was solubilized in 20 mM 4-(2-hydroxyethyl)-1-piperazineethanesulfonic acid buffer (pH 8) and 0.1% v/v Triton X-100. A stock solution of gelatin (0.1% w/v) was prepared using cholinesterase enzyme and human butyrylcholinesterase. First, the final concentration of DMSO ($\leq 1\%$ v/v) was prepared using the five inhibitor concentrations in ascending order, which showed inhibition in the range of at least 20–80%. Succinctly, following a 10 min preincubation period, 340 μM DTNB and 500 μM of the appropriate substrate butyrylthiocholine iodide (BTCI) for hBChE and acetylthiocholine iodide (ATCI) for hAChE were added to the mixture containing 25 μL of human AChE or BChE (0.25 U/mL) and 10 μL of the sample compound. Except for the enzyme that catalyzes the substrates, non-enzymatic hydrolysis blank readings were recorded for every scaffold. The Multimode Microplate Reader (BioTek Synergy

H1M, USA) was used to continuously monitor the change in absorbance reading at λ = 413 nm at 37 °C for a duration of 6 min. The inhibition percentage was computed using the formula $[(V_0 - V_i)/V_0] \times 100$, which involved comparing the reaction rate with and without inhibitors. The initial and final concentrations, with or without inhibitors, are represented by V_i and V_0 , which are the reaction rates. The nonlinear variable slope of the log (inhibitor) vs normalized was used to calculate the IC50 value for each sample compound (Graph Pad Prism 5.01).^{36,37} The assay was conducted in three different experiments in triplicate to validate the experimental results.

To ascertain the type of inhibition of human acetylcholinesterase and human butyrylcholinesterase, enzyme kinetics were estimated on the test compound, **5AD**, at six different concentrations of acetylthiocholine iodide or butyrylthiocholine iodide (60–400 μM).³⁸ Three different concentrations of the compound **5AD** (0.030, 0.060, 0.090 μM for AChE; and 0.100, 0.200, 0.300 μM for BChE) were taken for the experiments and estimated against all the six concentrations of substrates.³⁸ To see the kind of inhibition against hAChE and hBChE, a Lineweaver–Burk double reciprocal plot was created between various substrate concentrations and reaction rates.³⁹ In the end, the Dixon plot was used for calculation of K_i values.⁴⁰

A FRET-based fluorometric assay was utilized to ascertain the test scaffolds' BACE-1 inhibitory ability using the BACE-1 detection assay (CS0010, Sigma, India).⁴¹ This technique makes use of the idea that a higher fluorescence intensity results from BACE-1 cleavage. First, an assay mixture was created by mixing the substrate (20 μL), test scaffolds (2 μL), and fluorescent assay buffer (78 μL). Next, 2 μL of BACE-1 (0.3 U/ μL) was added. Next, the fluorescence intensity was measured at 405 nm for emission wavelengths and 320 nm for excitation wavelengths. The positive and negative controls with and without the enzyme were also estimated. To measure the fluorescence intensity, a blank was used as the negative control. Fluorescent intensities of test compounds were calculated in order to estimate the percentage inhibition following formula was used: $100 - (F_i/F_0 \times 100)$, where F_i is the observed fluorescence intensity when the inhibitor is present and F_0 is the recorded fluorescence intensity when the inhibitor is absent.⁴²

4.3. DPPH-Based Antioxidant Activity. The antioxidant potential of the synthesized derivatives (**5AD-5AI**) were performed using the method reported by Shaikh et al.⁴³ The test compound concentrations were prepared 100, 75, 50, and 25 μM in methanol. Similarly, DPPH 100 μM and ascorbic acid (100, 75, 50, 25 μM) concentrations were prepared in methanol. Equimolar concentration was added to each well and incubated for 30 min in a dark condition. A decrease in the absorption intensity was noted at 517 nm. Percentage radical scavenging assay was calculated using the formula F_i (absorbance intensity of inhibitor) – F_c (absorbance intensity of control)/ $F_c \times 100$.

4.4. Propidium Iodide Displacement Assay. The PI displacement assay was conducted to validate the binding between the experimental scaffolds and the peripheral active site (PAS) of human acetylcholinesterase (hAChE). PI is recognized as a significant ligand that binds prominently to the peripheral anionic site (PAS) of human acetylcholinesterase (hAChE). The comparative binding ability of the screened experimental scaffolds (**5AD**) and the standard (DNP) was assessed at this specific binding site. The experimental

scaffolds, prepared at concentrations of 10 or 50 μM , 150 μL , were first subjected to incubation at 25 $^{\circ}\text{C}$ for 6 h in the presence of hAChE (5U). Subsequently, 1 μM PI (50 μL) was introduced. The fluorescent intensity was measured ($\lambda_{\text{ex}} = 450$ nm, $\lambda_{\text{em}} = 485$ nm). The fluorescence intensities of both the test sample and the standard were quantified to determine the percentage of PI displacement in the presence or absence of the inhibitor.⁴⁴

4.5. Blood–Brain Barrier (BBB) Permeability Assay.

To assess the permeability of the blood–brain barrier for the test compounds and the conventional medication, donepezil was conducted following a previously documented procedure. The procedure involves the creation of a PVDF membrane with a coating applied, specifically for the acceptor microplate, with a pore size of 0.45 μm . The application of the coating was achieved by using lipid derived from porcine brain (4 μL , concentration: 20 mg/mL). The test scaffolds were solubilized in PBS (pH 7.4):EtOH (in a ratio of 7:3 v/v) to uphold the stock solution. In the donor microplates, 200 μL of the test scaffold solution was dispensed, followed by the addition of 200 μL of a solution containing PBS:EtOH (7:3 v/v) into the acceptor plate and incubated for 18 h at 25 $^{\circ}\text{C}$. The microplates were aligned in a suitable configuration and kept at a temperature of 25 $^{\circ}\text{C}$ for 18 h, enabling the transfer from donor plate to the acceptor plate via the PVDF membrane coated with lipid of the test compound. Spectrophotometrically, the concentration of test scaffold in the acceptor, donor, and reference plate was recorded.²⁵ Previously, the method was validated by commercially available nine drugs with known permeability across the BBB.⁴⁵

4.6. Estimation of $A\beta$ Aggregation: Thioflavin T Assay. Thioflavin T assay was used to study the inhibitory potential of test compound against aggregation of $A\beta$. The protein ($A\beta$) was dissolved in ammonium hydroxide (pH ≥ 9.0) to create $A\beta$ (2000 μM). For the test compounds, the stock solution was prepared in PBS (pH 7.4) and DMSO ($\leq 1\%$ w/v). Various concentrations of test compounds (5, 10, and 20 μM) were used.^{46,47} In the self-induced anti- $A\beta$ aggregation assay, thioflavin T (180 μL , 5 μM) solution was added to 50 mM glycine-NaOH buffer pH 8.0 after the mixture of $A\beta$ (10 μM) in PBS pH with or without inhibitor (different concentrations 5, 10, and 20 μM) was incubated (37 $^{\circ}\text{C}$, 48 h).⁴⁸ The fluorescent intensity was measured ($\lambda_{\text{ex}} = 450$ nm, $\lambda_{\text{em}} = 485$ nm). Anti- $A\beta$ aggregatory potential was calculated using a formula:

$$\% \text{inhibition} = [100 - (F_i/F_0 \times 100)] \text{ and } \text{NFI} = F_i/F_0$$

where F_i and F_0 are the fluorescence intensities with or without inhibitors, respectively.⁴⁹

To estimate hAChE-induced anti- $A\beta$ aggregation, the mixture of $A\beta$ (2 μL) and hAChE (16 μL) with or without test compounds at various concentrations 5, 10, and 20 μM was incubated for 48 h at 37 $^{\circ}\text{C}$. After that, thioflavin T (180 μL , 5 μM) solution in 50 mM glycine-NaOH buffer pH 8.0 was added, and the fluorescent intensity was measured ($\lambda_{\text{ex}} = 450$ nm, $\lambda_{\text{em}} = 485$ nm). The hAChE-induced anti- $A\beta$ aggregatory potential was calculated using the above equation.^{50,51}

4.7. In Vivo Studies. 4.7.1. Animals.

Adult Swiss albino mice weighing between 24 and 28 g were obtained from accredited suppliers. The experimental protocol, including the necessary number of mice, received approval from the Animal Ethical Committee under reference Dean/2017/CEC/92. The animals were housed in individual cages grouped accordingly

in a temperature-controlled room with controlled sound levels and a 12 h dark-light cycle, maintaining a temperature of 25 $^{\circ}\text{C}$. Mice were provided with unrestricted access to water and a balanced diet, although they underwent a 1 h fasting period before the experiments.

4.7.2. Acute Oral Toxicity Studies. Compound SAD underwent acute oral toxicity assessment following OECD guidelines 423. It was administered in graded doses reaching up to 100 mg/kg, and mice were continuously observed individually for behavioral and autonomic changes, including salivation, tremors, seizures, diarrhea, lethargy, and coma. These observations were monitored at intervals of 1, 3, 5, and 24 h postadministration, and subsequent mortality was recorded for a duration of 14 days.^{52,53}

4.7.3. Y-Maze Test for Spatial Learning Memory. The short-term cognitive behavior attenuation test for compound SAD was examined with the amnesia model in the Y-maze rodent model, which was produced by the scopolamine. Initially, 0.3% w/v sodium carbomethoxy cellulose (NaCMC) was used to make the suspension of the test compound. NaCMC acts as a surfactant to solubilize the test compound. Normal saline (NS) solution was used as a vehicle to make the solution of scopolamine (0.5 mg/kg). In total, 6 groups of Swiss albino mice were arranged and selected randomly. For further study, animals were bifurcated into the control group, scopolamine (0.5 mg/kg, i.p.), donepezil (5 mg/kg, po), and three test compound group (5, 10, and 20 mg/kg).

The anti-amnesic effect of test compounds was assessed using a Y-maze apparatus with three arms (A, B, and C) arranged at equal angles. Before each test, every arm was meticulously cleaned and wiped with alcohol for thorough sanitation. Each mouse was kept at the center of the inception point to three arms and allowed to move in all directions without any restraint. Similarly, all the groups were subjected to the same set of experiment to estimate percentage spontaneous alteration according to number of arm entries and calculated by using formula: [no. of spontaneous alterations/(total number of arm entries - 2)] \times 100.

4.8. Ex Vivo Studies and Biochemical Analysis.

Following the Y-maze experiment, all of the mouse groups were promptly euthanized through cervical dislocation. Subsequently, their brains were extracted from the skull and homogenized by using a glass homogenizer in 5 mL of 12.5 mM sodium phosphate buffer (pH 7.4). The resulting homogenates underwent centrifugation at 7000 rpm for 30 min at 4 $^{\circ}\text{C}$. The supernatants obtained after centrifugation were collected and employed for assessing various biochemical parameters.

The Ellman's colorimetric method, slightly modified, was employed to assess cholinergic biomarkers (AChE/BChE). Additionally, 100 μL of the obtained supernatant underwent a 5 min incubation with ATCI or BTCl (15 mM each in 100 μL). Following the incubation, 100 μL of 1.5 mM DTNB was introduced, and absorbances were concurrently measured at 415 nm.³⁵

MDA and CAT analyses were conducted to assess the antioxidant capabilities of the identified compound. The evaluation of MDA levels utilized the TBARS assay, which is a method also known as the lipid peroxidation assay. This assay relies on spectrophotometrically detecting a red TBARS compound, formed through the reaction between thiobarbituric acid and MDA under acidic conditions. For the experiment, 1.5 mL of 20% glacial acetic acid (GAA), 0.2 mL of 8% sodium

lauryl sulfate (SLS), and 1.5 mL of a 0.8% aqueous solution of thiobarbituric acid (TBA) were added to 0.2 mL of the processed brain homogenate. The mixture was then brought to a volume of 4.0 mL with deionized water and heated at 95 °C for 60 min. After cooling, 5 mL of a mixed solution of *n*-butanol and pyridine (15:1 v/v) with 1 mL of distilled water was added and centrifuged. The organic layer (200 μ L) was isolated in a 96-well plate, and absorbance was measured at 532 nm using a 96-well microplate reader.^{54,55}

Catalase (CAT) is a crucial enzyme responsible for catalyzing the breakdown of hydrogen peroxide (H₂O₂) into water and oxygen. The assessment of CAT activity followed the protocol outlined by Sinha. The assay mixture comprised 50 mM PBS (0.1 M; pH 7.4), 50 mL of 800 mM hydrogen peroxide (H₂O₂), 50 mM brain supernatant, and 100 mL of dichromate/acetic acid solution (5% K₂Cr₂O₇/glacial acetic acid; 1:3 v/v). In a 96-well plate, 50 mM brain supernatant, 50 mM PBS (0.1 M pH 7.4), and 50 mL of 800 mM hydrogen peroxide (H₂O₂) were incubated at 37 °C for 1 min. Following incubation, 150 mL of dichromate/acetic acid solution (coloring reagent) was added, and the mixture was boiled at 100 °C for 10 min. Subsequently, the absorbance was measured at 570 nm using a 96-well microplate reader.⁵⁶

4.9. Computational Studies. **4.9.1. Molecular Docking.** **4.9.1.1. Protein and Ligand Preparation.** To study the binding energy of the designed compounds on targets, AChE (PDB ID: 4EY7) and BACE-1 (PDB ID: 2ZJM). The Schrodinger Suite 2022–1 protein preparation wizard tool was utilized to prepare the protein. It consists of three essential steps: first, the OPLS-2005 force field was used to ascribe the partial charge after hydrogens were added. The same field was also used to ascribe the protonated states, and partial energy minimization was used to regulate the heavy atoms. By destruction of the ligand, the location for ligand binding was established. The next phase involved creating ligands using the LigPrep module with the OPLS-2005 force field and default settings.

4.9.1.2. Docking Analysis. A grid generating module program found in Schrodinger was used to create the grid that was used to dock the ligand. The prepared grid was validated by redocking the same ligand at the docking site. The glide docking default configuration of Schrodinger's XP module was used. The prior grid was used for docking, and the ligand that was generated via LigPrep was used. It was discovered that every structure fits inside the binding pocket, and each docking run's lowest energy position was maintained.

4.9.2. Pharmacokinetic Profiling using SwissADME Prediction Tool. The SwissADME prediction tool was used to estimate ADME properties, including physicochemical properties, pharmacokinetics, drug-likeness, and medicinal chemistry friendliness, among which in-house proficient methods such as the BOILEDegg, iLOGP, and Bioavailability Radar. All of the ligands were subjected to prediction of ADME properties.

4.9.3. Estimate Ligand Binding Affinity: MM/GBSA. The Prime module of the Schrodinger was utilized to evaluate the binding energy of the proposed test compounds acquired by XP docking for AChE & BACE-1 inhibitors using the Molecular Mechanics-Generalized Born Surface Area (MM-GBSA) tool. The docked complex's "out.maegz" file from XP docking was utilized in the module to rank the compounds according to their predicted binding energies.⁵⁷

4.9.4. Molecular Simulations Studies. The binding stability and binding paradigm of the docked ligand-hAChE/BACE-1

complexes were asserted by molecular simulation using the Desmond module. The environment of the docked complexes was established by generating a TIP3P water model used for additional solvation of the system, which was counteracted by inclusion of counterions. The steady temperature (300 K) and pressure (1.01325 bar) were maintained throughout the simulation. Simulation was done for 100 ns.

■ ASSOCIATED CONTENT

SI Supporting Information

The Supporting Information is available free of charge at <https://pubs.acs.org/doi/10.1021/acsomega.3c10276>.

Characterization data (FT-IR, ¹H NMR, ¹³C NMR, and HRMS) and in silico data including docking studies and SwissADME results (PDF)

■ AUTHOR INFORMATION

Corresponding Author

Sushant K. Shrivastava – Pharmaceutical Chemistry Research Laboratory, Department of Pharmaceutical Engineering & Technology, Indian Institute of Technology, (Banaras Hindu University), Varanasi 221005, India; orcid.org/0000-0002-5500-4004; Email: skshrivastava.phe@itbhu.ac.in

Authors

Abhinav Singh – Pharmaceutical Chemistry Research Laboratory, Department of Pharmaceutical Engineering & Technology, Indian Institute of Technology, (Banaras Hindu University), Varanasi 221005, India

Akash Verma – Pharmaceutical Chemistry Research Laboratory, Department of Pharmaceutical Engineering & Technology, Indian Institute of Technology, (Banaras Hindu University), Varanasi 221005, India

Bhagwati Bhardwaj – Pharmaceutical Chemistry Research Laboratory, Department of Pharmaceutical Engineering & Technology, Indian Institute of Technology, (Banaras Hindu University), Varanasi 221005, India

Poorvi Saraf – Pharmaceutical Chemistry Research Laboratory, Department of Pharmaceutical Engineering & Technology, Indian Institute of Technology, (Banaras Hindu University), Varanasi 221005, India

Hansal Kumar – Pharmaceutical Chemistry Research Laboratory, Department of Pharmaceutical Engineering & Technology, Indian Institute of Technology, (Banaras Hindu University), Varanasi 221005, India

Nishi Jain – Pharmaceutical Chemistry Research Laboratory, Department of Pharmaceutical Engineering & Technology, Indian Institute of Technology, (Banaras Hindu University), Varanasi 221005, India

Digambar Kumar Waiker – Pharmaceutical Chemistry Research Laboratory, Department of Pharmaceutical Engineering & Technology, Indian Institute of Technology, (Banaras Hindu University), Varanasi 221005, India

T A Gajendra – Neurotherapeutics Research Laboratory, Department of Pharmaceutical Engineering & Technology, Indian Institute of Technology, (Banaras Hindu University), Varanasi 221005, India

Sairam Krishnamurthy – Neurotherapeutics Research Laboratory, Department of Pharmaceutical Engineering & Technology, Indian Institute of Technology, (Banaras Hindu University), Varanasi 221005, India

Complete contact information is available at:

<https://pubs.acs.org/10.1021/acsomega.3c10276>

Author Contributions

A.S. helped with conceptualization, methodology, and writing of the original draft, review, and editing. A.V. helped with in vitro studies and investigations. B.B. carried out in silico studies. P.S. helped in writing manuscript draft. H.K., D.K.W., and N.J. helped in curation of chemistry related concepts. T.A.G. helped in performing in vivo and ex vivo studies. S.K. helped in writing the original draft, editing, and review. S.K.S. helped with conceptualization, editing, and review.

Notes

The authors declare no competing financial interest.

ACKNOWLEDGMENTS

The authors show gratitude toward Central Instrument Facility for NMR experiments and Param Shivay Supercomputing Centre for computational studies. Authors are also thankful to Indian Council of Medical Research for providing financial assistance through Extramural Ad-hoc approval (File no. 52/11/2020-BIO/BMS).

REFERENCES

- (1) Guo, T.; Zhang, D.; Zeng, Y.; Huang, T. Y.; Xu, H.; Zhao, Y. Molecular and cellular mechanisms underlying the pathogenesis of Alzheimer's disease. *Mol. Neurodegener.* **2020**, *15* (1), 40.
- (2) Ballard, C.; Gauthier, S.; Corbett, A.; Brayne, C.; Aarsland, D.; Jones, E. J. Alzheimer's disease. *Lancet (London, England)* **2011**, *377* (9770), 1019–1031.
- (3) Scheltens, P.; De Strooper, B.; Kivipelto, M.; Holstege, H.; Chételat, G.; Teunissen, C. E.; Cummings, J.; van der Flier, W. M. Alzheimer's disease. *Lancet (London, England)* **2021**, *397* (10284), 1577–1590.
- (4) Hardy, J. A.; Higgins, G. A. J. S. Alzheimer's disease: the amyloid cascade hypothesis. *Science (New York, N.Y.)* **1992**, *256* (5054), 184–185.
- (5) Maccioni, R. B.; Fariás, G.; Morales, I.; Navarrete, L. J. The revitalized tau hypothesis on Alzheimer's disease. *Arch. Med. Res.* **2010**, *41* (3), 226–231.
- (6) Wang, R.; Reddy, P. H. Role of glutamate and NMDA receptors in Alzheimer's disease. *J. Alzheimer's Dis.* **2017**, *57* (4), 1041–1048.
- (7) Lucas, S. M.; Rothwell, N. J.; Gibson, R. M. The role of inflammation in CNS injury and disease. *Br. J. Pharmacol.* **2006**, *147* (S1), S232–S240.
- (8) Saura, C. A.; Valero, J., The role of CREB signaling in Alzheimer's disease and other cognitive disorders. *Rev. Neurosci.* **2011**.
- (9) Cummings, J.; Lee, G.; Nahed, P.; Kambh, M. E. Z. N.; Zhong, K.; Fonseca, J.; Taghva, K. J. A. s.; Research, D. T.; Interventions, C. Alzheimer's disease drug development pipeline. *Alzheimer's & dementia (New York, N. Y.)* **2022**, *8* (1), 12295.
- (10) Mangialasche, F.; Solomon, A.; Winblad, B.; Mecocci, P.; Kivipelto, M. Alzheimer's disease: clinical trials and drug development. *Lancet. Neurol.* **2010**, *9* (7), 702–716.
- (11) Bajda, M.; Guzior, N.; Ignasik, M.; Malawska, B. J. C. m. c. Multi-target-directed ligands in Alzheimer's disease treatment. *Curr. Med. Chem.* **2011**, *18* (32), 4949–4975.
- (12) Gulcan, H. O.; Kosar, M. The Hybrid Compounds as Multi-target Ligands for the Treatment of Alzheimer's Disease: Considerations on Donepezil. *Curr. Top Med. Chem.* **2022**, *22* (5), 395–407.
- (13) Mishra, P.; Kumar, A.; Panda, G. Anti-cholinesterase hybrids as multi-target-directed ligands against Alzheimer's disease (1998–2018). *Bioorg. Med. Chem.* **2019**, *27* (6), 895–930.
- (14) Sinha, S. K.; Shrivastava, S. K. Design, synthesis and evaluation of some new 4-aminopyridine derivatives in learning and memory. *Bioorg. Med. Chem. Lett.* **2013**, *23* (10), 2984–2989.
- (15) Tripathi, P. N.; Srivastava, P.; Sharma, P.; Tripathi, M. K.; Seth, A.; Tripathi, A.; Rai, S. N.; Singh, S. P.; Shrivastava, S. K. Biphenyl-3-oxo-1, 2, 4-triazine linked piperazine derivatives as potential cholinesterase inhibitors with anti-oxidant property to improve the learning and memory. *Bioorg. Chem.* **2019**, *85*, 82–96.
- (16) Mishra, C. B.; Kumari, S.; Manral, A.; Prakash, A.; Saini, V.; Lynn, A. M.; Tiwari, M. Design, synthesis, in-silico and biological evaluation of novel donepezil derivatives as multi-target directed ligands for the treatment of Alzheimer's disease. *Eur. J. Med. Chem.* **2017**, *125*, 736–750.
- (17) Shrivastava, S. K.; Sinha, S. K.; Srivastava, P.; Tripathi, P. N.; Sharma, P.; Tripathi, M. K.; Tripathi, A.; Choubey, P. K.; Waiker, D. K.; Aggarwal, L. M.; Dixit, M.; Kheruka, S. C.; Gambhir, S.; Shankar, S.; Srivastava, R. K. Design and development of novel p-aminobenzoic acid derivatives as potential cholinesterase inhibitors for the treatment of Alzheimer's disease. *Bioorg. Chem.* **2019**, *82*, 211–223.
- (18) Kennedy, M. E.; Stamford, A. W.; Chen, X.; Cox, K.; Cumming, J. N.; Dockendorf, M. F.; Egan, M.; Ereshefsky, L.; Hodgson, R. A.; Hyde, L. A. The BACE1 inhibitor verubecestat (MK-8931) reduces CNS β -amyloid in animal models and in Alzheimer's disease patients. *Sci. Transl. Med.* **2016**, *8* (363), 363–150.
- (19) Rao, P. P.; Pham, A. T.; Shakeri, A. J. S. M. D. D. M., Molecules; Applications, Discovery of small molecules for the treatment of Alzheimer's. *SMDD* **2019**, 289.
- (20) Elghazawy, N. H.; Zaafar, D.; Hassan, R. R.; Mahmoud, M. Y.; Bedda, L.; Bakr, A. F.; Arafa, R. K. J. Discovery of new 1, 3, 4-oxadiazoles with dual activity targeting the cholinergic pathway as effective anti-Alzheimer agents. *ACS Chem. Neurosci.* **2022**, *13* (8), 1187–1205.
- (21) Tripathi, A.; Choubey, P. K.; Sharma, P.; Seth, A.; Tripathi, P. N.; Tripathi, M. K.; Prajapati, S. K.; Krishnamurthy, S.; Shrivastava, S. K. Design and development of molecular hybrids of 2- pyridyl piperazine and 5-phenyl-1, 3, 4-oxadiazoles as potential multifunctional agents to treat Alzheimer's disease. *Eur. J. Med. Chem.* **2019**, *183*, No. 111707.
- (22) Pancechowsak-Ksepko, D.; Foks, H.; Janowiec, M.; Zwolska-Kwiek, Z. J. A. P. P. Synthesis and tuberculostatic activity of reaction products 5-(2-, 3-and 4-pyridil)-1, 3, 4-oxadiazol-2-thione with amines. *Acta Polym. Pharm.* **1993**, *50* (2–3), 259–267.
- (23) Rahim, F.; Javed, M. T.; Ullah, H.; Wadood, A.; Taha, M.; Ashraf, M.; Khan, M. A.; Khan, F.; Mirza, S.; Khan, K. M. Synthesis, molecular docking, acetylcholinesterase and butyrylcholinesterase inhibitory potential of thiazole analogs as new inhibitors for Alzheimer disease. *Bioorg. Chem.* **2015**, *62*, 106–116.
- (24) Waiker, D. K.; Verma, A.; Akhilesh, A. G. T.; Singh, N.; Roy, A.; Dilmashin, H.; Tiwari, V.; Trigun, S. K.; Singh, S. P.; Krishnamurthy, S.; Lama, P.; Davison, V. J.; Shrivastava, S. K. Design, Synthesis, and Biological Evaluation of Piperazine and N-Benzylpiperidine Hybrids of 5-Phenyl-1,3,4- oxadiazol-2-thiol as Potential Multitargeted Ligands for Alzheimer's Disease Therapy. *ACS Chem. Neurosci.* **2023**, *14* (11), 2217–2242.
- (25) Di, L.; Kerns, E. H.; Fan, K.; McConnell, O. J.; Carter, G. T. High throughput artificial membrane permeability assay for blood–brain barrier. *Eur. J. Med. Chem.* **2003**, *38* (3), 223–232.
- (26) Palmer, T.; Jamson, L.-M.; Shelley, L.; James, R. Propidium—a Fluorescence Probe for a Peripheral Anionic Site on Acetylcholinesterase. *Mol. Pharm.* **1974**, *10* (4), 703.
- (27) Klinkenberg, I.; Blokland, A. The validity of scopolamine as a pharmacological model for cognitive impairment: a review of animal behavioral studies. *Neurosci. & Biobehav. Rev.* **2010**, *34* (8), 1307–1350.
- (28) Lalonde, R. The neurobiological basis of spontaneous alternation. *Neurosci. & Biobehav. Rev.* **2002**, *26* (1), 91–104.
- (29) Ellman, G. L.; Courtney, K. D.; Andres, V., Jr; Featherstone, R. M. A new and rapid colorimetric determination of acetylcholinesterase activity. *Biochem. Pharmacol.* **1961**, *7* (2), 88–95.
- (30) Bonda, D. J.; Wang, X.; Perry, G.; Nunomura, A.; Tabaton, M.; Zhu, X.; Smith, M. A. Oxidative stress in Alzheimer disease: a

possibility for prevention. *Neuropharmacol.* **2010**, *59* (4–5), 290–294.

(31) Daina, A.; Michielin, O.; Zoete, V. J. SwissADME: a free web tool to evaluate pharmacokinetics, drug-likeness and medicinal chemistry friendliness of small molecules. *Sci. Rep.* **2017**, *7* (1), 42717.

(32) Lagunin, A. A.; Dubovskaja, V. I.; Rudik, A. V.; Pogodin, P. V.; Druzhilovskiy, D. S.; Glorizova, T. A.; Filimonov, D. A.; Sastry, N. G.; Porokov, V. V. CLC-Pred: A freely available webservice for in silico prediction of human cell line cytotoxicity for drug-like compounds. *PLoS One* **2018**, *13* (1), No. 0191838.

(33) Goher, S. S.; Griffett, K.; Hegazy, L.; Elagawany, M.; Arief, M. M.; Avdagic, A.; Banerjee, S.; Burris, T. P.; Elgendy, B. J. B. Development of novel liver X receptor modulators based on a 1, 2, 4-triazole scaffold. *Bioorg. Med. Chem. Lett.* **2019**, *29* (3), 449–453.

(34) Zhang, K.; Wang, P.; Xuan, L.-N.; Fu, X.-Y.; Jing, F.; Li, S.; Liu, Y.-M.; Chen, B.-Q. J. B. Synthesis and antitumor activities of novel hybrid molecules containing 1, 3, 4-oxadiazole and 1, 3, 4-thiadiazole bearing Schiff base moiety. *Bioorg. Med. Chem. Lett.* **2014**, *24* (22), 5154–5156.

(35) Ellman, G. L.; Courtney, K. D.; Andres, V., Jr; Featherstone, R. M. J. A new and rapid colorimetric determination of acetylcholinesterase activity. *Biochem. Pharmacol.* **1961**, *7* (2), 88–95.

(36) Peauger, L.; Azzouz, R.; Gembus, V.; Tintas, M.-L.; Sopková-de Oliveira Santos, J.; Bohn, P.; Papamicael, C.; Levacher, V. J. Donepezil-based central acetylcholinesterase inhibitors by means of a “bio-oxidizable” prodrug strategy: design, synthesis, and in vitro biological evaluation. *J. Med. Chem.* **2017**, *60* (13), 5909–5926.

(37) Waiker, D. K.; Verma, A.; Saraf, P.; TA, G.; Krishnamurthy, S.; Chaurasia, R. N.; Shrivastava, S. K. Development and Evaluation of Some Molecular Hybrids of N-(1-Benzylpiperidin-4-yl)-2-((5-phenyl-1, 3, 4-oxadiazol-2-yl) thio) as Multifunctional Agents to Combat Alzheimer’s Disease. *ACS Omega*, **2023**.

(38) Lineweaver, H.; Burk, D. J. The determination of enzyme dissociation constants. *J. Am. Chem. Soc.* **1934**, *56* (3), 658–666.

(39) Lineweaver, H.; Burk, D.; Deming, W. E. The dissociation constant of nitrogen-nitrogenase in *Azotobacter*. *J. Am. Chem. Soc.* **1934**, *56* (1), 225–230.

(40) Dixon, M. J. The graphical determination of Km and Ki. *Biochem. J.* **1972**, *129* (1), 197–202.

(41) Prostack, L.; Barnea, E. J. S. S. A. USA., Sigma-Aldrich, P. Y., Zharhary, D., BACE1 activity assay kit (fluorescent).

(42) Gurjar, A. S.; Andrisano, V.; Simone, A. D.; Velingkar, V. S. Design, synthesis, in silico and in vitro screening of 1, 2, 4-thiadiazole analogues as non-peptide inhibitors of beta-secretase. *Bioorg. Chem.* **2014**, *57*, 90–98.

(43) Shaikh, S.; Pavale, G.; Dhavan, P.; Singh, P.; Uparkar, J.; Vaidya, S. P.; Jadhav, B. L.; Ramana, M. M. V. Design, synthesis and evaluation of dihydropyranoindole derivatives as potential cholinesterase inhibitors against Alzheimer’s disease. *Bioorg. Chem.* **2021**, *110*, No. 104770.

(44) Ramrao, S. P.; Verma, A.; Waiker, D. K.; Tripathi, P. N.; Shrivastava, S. K. Design, synthesis, and evaluation of some novel biphenyl imidazole derivatives for the treatment of Alzheimer’s disease. *J. Mol. Struct.* **2021**, *1246*, No. 131152.

(45) Seth, A.; Sharma, P. A.; Tripathi, A.; Choubey, P. K.; Srivastava, P.; Tripathi, P. N.; Shrivastava, S. K. Design, synthesis, evaluation and molecular modeling studies of some novel N substituted piperidine-3-carboxylic acid derivatives as potential anticonvulsants. *Med. Chem. Res.* **2018**, *27*, 1206–1225.

(46) LeVine, H., III Quantification of β -sheet amyloid fibril structures with thioflavin T. *Meth. Enzymol.* **1999**, *309*, 274–284.

(47) Hudson, S. A.; Ecroyd, H.; Kee, T. W.; Carver, J. A. The thioflavin T fluorescence assay for amyloid fibril detection can be biased by the presence of exogenous compounds. *FEBS J.* **2009**, *276* (20), 5960–5972.

(48) Bolder, S. G.; Sagis, L. M.; Venema, P.; van der Linden, E. Thioflavin T and birefringence assays to determine the conversion of proteins into fibrils. *Langmuir: ACS J. Sur. Coll.* **2007**, *23* (8), 4144–4147.

(49) Rajasekhar, K.; Madhu, C.; Govindaraju, T. J. Natural tripeptide-based inhibitor of multifaceted amyloid β toxicity. *ACS Chem. Neurosci.* **2016**, *7* (9), 1300–1310.

(50) Bolognesi, M. L.; Cavalli, A.; Valgimigli, L.; Bartolini, M.; Rosini, M.; Andrisano, V.; Recanatini, M.; Melchiorre, C. J. Multi-target-directed drug design strategy: from a dual binding site acetylcholinesterase inhibitor to a trifunctional compound against Alzheimer’s disease. *J. Med. Chem.* **2007**, *50* (26), 6446–6449.

(51) Shidore, M.; Machhi, J.; Shingala, K.; Murumkar, P.; Sharma, M. K.; Agrawal, N.; Tripathi, A.; Parikh, Z.; Pillai, P.; Yadav, M. R. Benzylpiperidine-linked diarylthiazoles as potential anti-Alzheimer’s agents: synthesis and biological evaluation. *J. Med. Chem.* **2016**, *59* (12), 5823–5846.

(52) Jonsson, M.; Jestoi, M.; Nathanail, A. V.; Kokkonen, U.-M.; Anttila, M.; Koivisto, P.; Karhunen, P.; Peltonen, K. J. Application of OECD Guideline 423 in assessing the acute oral toxicity of moniliformin. *Food Chem. Toxicol.* **2013**, *53*, 27–32.

(53) Bedi, O.; Krishan, P. J. Investigations on acute oral toxicity studies of purpurin by application of OECD guideline 423 in rodents. *Naunyn-Schmiedeberg’s Arch. Pharmacol.* **2020**, *393*, 565–571.

(54) Senthilkumar, M.; Amaresan, N.; Sankaranarayanan, A.; Senthilkumar, M.; Amaresan, N.; Sankaranarayanan, A. *Estimation of malondialdehyde (MDA) by thiobarbituric acid (TBA) assay*. Springer: 2021.

(55) Khoubnasabjafari, M.; Ansarin, K.; Jouyban, A. J. Reliability of malondialdehyde as a biomarker of oxidative stress in psychological disorders. *BioImpacts* **2015**, *5* (3), 123.

(56) Ansari, M. A.; Scheff, S. W.; Neurology, E. Oxidative stress in the progression of Alzheimer disease in the frontal cortex. *J. Neuropathol. Exp. Neurol.* **2010**, *69* (2), 155–167.

(57) Hou, T.; Wang, J.; Li, Y.; Wang, W. J. modeling, Assessing the performance of the MM/PBSA and MM/GBSA methods. 1. The accuracy of binding free energy calculations based on molecular dynamics simulations. *J. Chem. Info. Model.* **2011**, *51* (1), 69–82.